The interplay of energy consumption and catalyst load in steam-reforming efficiency

Mauro Fernandes Pereira[a], Jorge P. Zubelli[b], Renan de S. Teixeira[c]

[a]*Department of Condensed Matter Theory, Institute of Physics CAS, 182 21 Prague, Czech Republic*
[b]*IMPA, Est. D. Castorina, 110, Jardim Botânico, Rio de Janeiro, 22460-320, Brazil*
[c]*Mathematics Department, UFRRJ, Br-465, Km 7, Seropédica, Rio de Janeiro, 23897-000, Brazil*

August 2019

Abstract

Catalysis consumes a large amount of energy and natural resources globally. Notably, the MIDREX (R) catalytic reform process delivers 60% of the world's iron production out of naturally occurring iron oxide, as of 2017. However, there are two outstanding questions regarding catalytic processes for which this paper delivers efficient answers: (i) How to solve the energy/catalyst investment dichotomy, i.e. locations with relatively inexpensive energy require less catalyst and in the opposite case of high energy costs, more catalyst is needed. (ii) How to express the energy input, which is difficult to ascertain for large burner designs, in terms of an easily measurable parameters in real time, such as a the input temperatures. These questions are unambiguously answered by our approach, which is coupled with an easily visualizable graphical solution, leading to a powerful design tool for catalytic processes in general, with huge potential to mitigate environmental impacts.

Keywords: Catalytic Reforming, Energy Efficiency, Nonlinear PDEs, Implicit-explicit algorithms, Reaction-diffusion equations.

Graphical Abstract

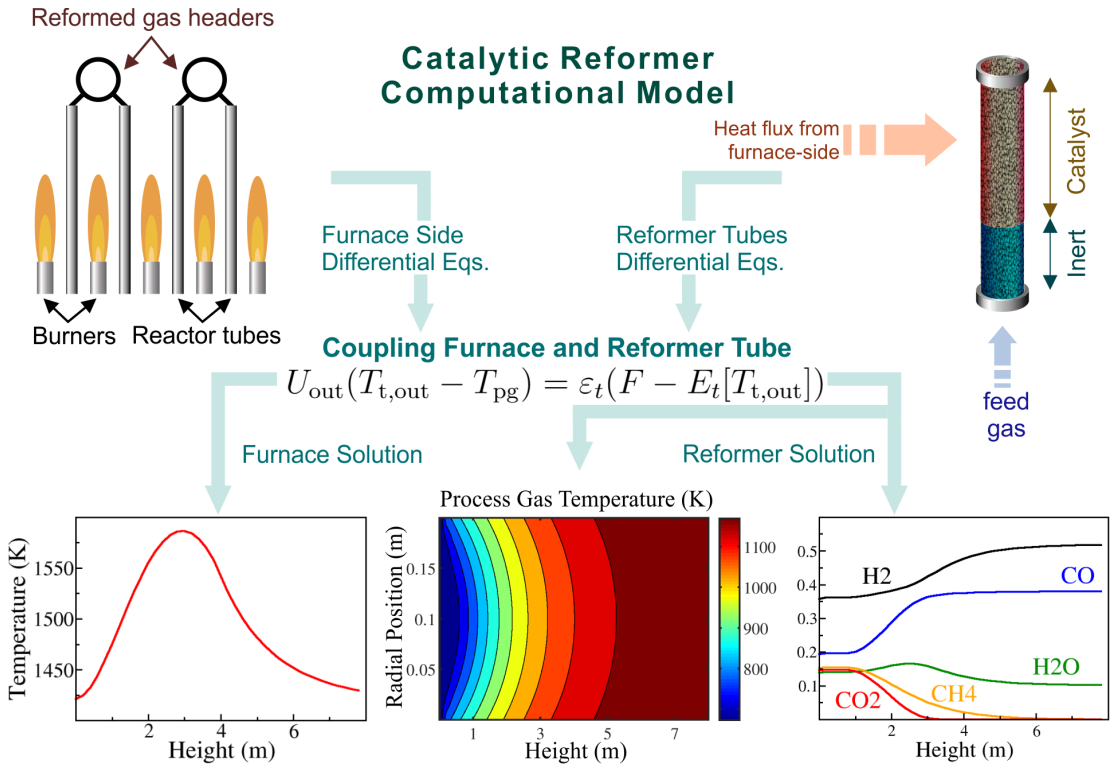

Highlights

1. Direct path to cost-benefit estimates of expenditures in both energy and catalyst.
2. Inputs defined by fully measurable temperatures and not by a hard-to-measure heat input flux.
3. Flexible and modular computational implementation capable of incorporating different material parameters and respecting the multiphysics and thermodynamic problem characteristics.
4. Highly applicable methodology to design energy efficient steam reformer systems by means of optimization techniques.
5. State of the art Implicit-Explicit algorithms are used to solve the stiff differential equation systems that model the temperature and concentration distributions.

Keywords: Catalytic Reforming, MIDREX (R) Process, Energy Efficiency, Computational Models and Heat Transfer.

1. Introduction

Industrial processes requiring catalysts in natural-gas steam reformers are one of the key large-scale technologies worldwide comprising a broad spectrum of applications ranging from traditional petrochemical industry to sustainable-energy technologies. Indeed, back in 1994, Rostrup-Nielsen [1] already strongly highlighted the increasing role of catalysis in large-scale conversion of natural gas for the energy and chemical sectors. Gas reforming plays a key role in the industrial production of hydrogen. As a matter of fact, 95% of the US-produced hydrogen comes from natural gas reforming plants [2]. The underlying method developed in this paper and applied to the steam reform and water gas reactions, has strong potential to impact on the design and further understanding of sustainable energy process such as: hybrid power generation with a new generation of catalyst materials, [3]; coproduction of electrical power and synthesis gas from biohythane [4]; proton conducting solid oxide fuel cells with internal methane steam reforming [5] and in numerous others. On the traditional iron industry side, the MIDREX (R) process is one of the most used siderurgical processes for direct reduction of iron ore. As of 2017, it was responsible for 60% of the world production of pre-reduced iron ore [6, 7], which is the path to steel production with massive impact on the environment, since the world steel production alone is responsible to 6% of anthropogenic CO2 emissions [8]. Modelling such processes is well known and is a crucial step for the design of major research and industrial units. However, there are two outstanding questions regarding catalytic processes for which this paper delivers efficient answers: (i) How to solve the energy/catalyst investment dichotomy, i.e. locations with relatively inexpensive energy require less catalyst and in the opposite case of high energy costs, more catalyst is needed. (ii) How to express the energy input, which is difficult to ascertain for large burner designs, in terms of an easily measurable parameters in real time, such as a the input temperatures, leading to a direct control of the process. These questions are unambiguously answered by our approach, which is based on state of the art Implicit-Explicit algorithms [9, 10, 11, 12] to solve the stiff differential equation systems describing the temperature and concentration distributions, coupled

with an easily visualizable graphical solution for the energy/catalyst dichotomy. Our approach is concretely illustrated by a numerical study of the MIDREX problem and can be automatically adapted to any catalytic process for which the underlying chemical reactions are known, leading to a powerful design tool for catalytic processes in general, with huge potential to mitigate environmental impacts. The Graphical Abstract summarizes the catalytic reformer computational model employed and some of the numerical results obtained.

2. Mathematical Model

A number of authors have developed models for the simulation of steam reformers. See the work of [13, 14, 15] and references therein. Regardless of all numerical progress achieved so far, there are outstanding issues, for which we deliver solutions here.

One of the key difficulties addressed in our approach is the fact that we are working with a system composed by two complex parts. The external one, which consists of a furnace where methane gas is burned to provide heat for the catalytic reaction that happens in the interior of the tubes. The internal one, through which CO_2 is converted to CO and steam. Both systems, which are nonlinear in nature, are coupled through the boundary of the tubes. Figure 1, following Ref. [7], shows a diagram of the MIDREX reformer tube considered in the numerical results delivered in this report. The issue here is that the solution requires iteration between the two compartments until convergence of a pair of strongly nonlinear equations with possible stiff behavior, which typically leads to instabilities and numerical error. The instabilities, in our case, are avoided by implementing a numerical solution of the coupled chemical and thermal problem with a third-order IMEX-SSP3(3,3,2) L-stable scheme [16, 11]. Another difficulty lies in the fact that many solution methods require knowledge of the heat input flux, which is very hard to measure in practice [7]. Our approach uses a directly measurable temperature to define the input of the problem and deliver a calibration curve and simple expression connecting this temperature with heat input. The procedure used for simulating the MIDREX steam reformer leading to the concentration of gases inside the reactor, necessary for the study of efficient

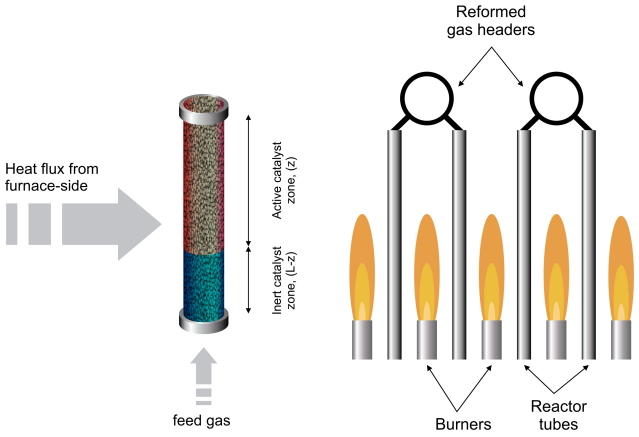

Figure 1: Schematics of a reformer tube and of the furnace.

production of CO_2 was developed by coupling the reactor-side model with the furnace-side model using an iterative process [13, 14, 15]. The furnace-side and reactor-side equations are solved separately for an initial guess $T_{\mathrm{t,out}}$ tube-skin temperature (K). It connects the heat flux between the oven and the reactor tubes. Then, the new value for the tube-skin temperature $T_{\mathrm{t,out}}$ can be calculated by making an energy balance on the tubes:

$$U_{\mathrm{out}}(T_{\mathrm{t,out}} - T_{\mathrm{pg}}) = \varepsilon_t(F - E_t[T_{\mathrm{t,out}}]). \tag{1}$$

Here, T_{pg} is the process gas temperature (K), F is the furnace half-sum of forward and backward axial heat flux (Wm^{-2}), and E_t is the black-body emissive power, which depends on $T_{\mathrm{t,out}}$. The overall heat transfer coefficient is denoted by U_{out}. Convergence is assumed to have been achieved whenever the relative error between two sequential steps is less than the convergence criterion (10^{-03}). In most of the approaches available, including Shayegan et al.[7], the flame energy q_0 is required. Unfortunately, it is usually not available from observed data.

We have thus introduced a crucial innovation by developing a way of estimating such value by using more easily measurable temperatures: $T_{\mathrm{fg},out} \equiv$ flue gas temperature (in K) at the output; $T_{\mathrm{fg},in} \equiv$ flue gas temperature (in K) at the input; $\overline{\Delta T} \equiv$ average temperature of the tube outer skin $-$ average temperature of the flue gas; $\overline{T_{\mathrm{fg}}} \equiv$; average flue gas temperature

in the furnace. Note that the value of $\overline{\Delta T}$ is typically negative because the temperature of the flue gas is above the the temperature of the tube. Based on such quantities and a series of approximations described step by step in the next paragraphs, we get the following value for q_o:

$$q_0 \approx c_{fg} G_{fg} (T_{\mathrm{f}g,out} - T_{\mathrm{f}g,in}) + \frac{8\sigma K_a \epsilon_t A_t L}{\beta} \quad \overline{\Delta T} \quad 4\overline{T_{\mathrm{f}g}}^3 \ . \tag{2}$$

A detailed numerical study also given below allows the expression of the energy input in terms of the combustion outlet temperature, $\overline{T_{\mathrm{f}g}}$, which is easily measured by sensors.

This shows how to use our algorithms as a calibration tool for the system, which can be easily extended for other catalyst processes. As an analogy, every heater at home or industry is controlled by the target temperature and not by the actual energy used (which ultimately leads to an electric or gas bill).

Furthermore, our method leads to a flexible and modular computational implementation. It is capable of incorporating different material parameters while respecting the multiphysics and thermodynamical problem characteristics.

In addition, we have developed an iterative scheme to calculate target CO_2 concentrations depicted in Figures 5 and 8. This allows a study of the interplay between the energy injected in the system and the amount of catalyst. For each combination of gas inlet temperature in the reactor, catalyst density and/or length along the tube and flame energy, we start a new convergence process for the tube-skin temperature, $T_{\mathrm{t,out}}$.

2.1. Reactor-Side Modelling

The chemical reactions that take place on catalytic steam reformers are complex and involve a number of chemical elements. Following [17] we have adopted the following three equations to model the problem:

$$CH_4 + H_2O \leftrightarrow 3H_2 + CO \tag{3a}$$

$$CO + H_2O \leftrightarrow H_2 + CO_2 \tag{3b}$$

$$CH_4 + 2H_2O \leftrightarrow 4H_2 + CO_2 \tag{3c}$$

The methodology we employed could be easily extended to more reactions if deemed necessary.

The reactor side is described by solving energy and mass balance equations for the two major components of reactant conversion ratio (x) and the temperature (T_{pg}). All equations operate under a steady-state condition in time. Thus the model for the reaction driven by a catalyst density distribution ρ_B inside each tube of Figure 1 is given by:

$$\frac{\partial x_{CH_4}}{\partial z} = \frac{D_{er}\rho_{pg}}{G_{pg}}\left[\frac{1}{r}\frac{\partial x_{CH_4}}{\partial r} + \frac{\partial^2 x_{CH_4}}{\partial r^2}\right] + \frac{\rho_B r_i \eta_i M_w}{G_{pg} y_{CH_4}} \tag{4}$$

$$\frac{\partial x_{CO_2}}{\partial z} = \frac{D_{er}\rho_{pg}}{G_{pg}}\left[\frac{1}{r}\frac{\partial x_{CO_2}}{\partial r} + \frac{\partial^2 x_{CO_2}}{\partial r^2}\right] - \frac{\rho_B r_i \eta_i M_w}{G_{pg} y_{CH_4}}, \tag{5}$$

and

$$G_{pg} c_{p,pg} \frac{\partial T_{pg}}{\partial z} = \left[\lambda_{er}\left(\frac{1}{r}\frac{\partial T_{pg}}{\partial r} + \frac{\partial^2 T_{pg}}{\partial r^2}\right) + \rho_B\left(\sum_{i=1}^{2}(-\Delta H_i) r_i \eta_i\right)\right]. \tag{6}$$

Here, ΔH_i are heats of reaction, ρ_{pg} is the process gas density, D_{er} is the effective radial diffusivity, λ_{er} is the effective radial conductivity, y_i is the molar fraction related to each gas component, M_w is the molar weight, $c_{p,pg}$ is the specific heat at constant pressure of the process gas and

$$G_{pg} = \frac{F_{fr} M_w}{N_t S_t}, \tag{7}$$

where F_{fr} is the feed gas flow rate. Furthermore, N_t is the number of the reactor tubes and S_t is the reactor tube cross section area. The variables r_i denote the reaction rates and η_i the effectiveness factor described in [18] and [19], respectively. The initial condition at the inlet of the reactor is:

$$x_{CO_2} = 0, \qquad x_{CH_4} = 0, \qquad T_{pg} = T_{feed} \qquad \text{and} \qquad P_{pg} = P_{feed}\ . \tag{8}$$

This choice of initial conditions can easily be changed if different combinations of the input gas are chosen.

The tube boundary conditions are:

$$\begin{aligned} \left.\frac{\partial x_{CH_4}}{\partial r}\right|_{r=0} &= 0 \qquad \text{and} \qquad \left.\frac{\partial x_{CH_4}}{\partial r}\right|_{r=r_{max}} = 0, \\ \left.\frac{\partial x_{CO_2}}{\partial r}\right|_{r=0} &= 0 \qquad \text{and} \qquad \left.\frac{\partial x_{CO_2}}{\partial r}\right|_{r=r_{max}} = 0, \\ \left.\frac{\partial T_{pg}}{\partial r}\right|_{r=0} &= 0 \qquad \text{and} \qquad \lambda_{er}\left.\frac{\partial T_{pg}}{\partial r}\right|_{r=r_{max}} = U_{in}(T_{out} - T_{pg}), \end{aligned} \tag{9}$$

where the overall heat transfer coefficient is based on the geometry and thermal properties of the reactor's surfaces:

$$\frac{1}{U_{in}} = \left(\frac{d_{t,in}}{2k_t}\ln\frac{d_{t,out}}{d_{t,in}} + \frac{1}{h_{fw}}\right). \tag{10}$$

Here, $d_{t,in}$ and $d_{t,out}$ are, respectively the internal and external tube diameters, k_t is the thermal conductivity of the tube material. and h_{fw} is the fluid wall heat transfer coefficient [20].

An extension of Ergun's equation was used to estimate the pressure (Pa) drop under high Reynolds numbers:

$$-\frac{\mathrm{d}p}{\mathrm{d}z} = f\frac{\rho_{pg}u_{pg}^2}{d_p} \qquad \text{and} \qquad f = \frac{1-\upsilon}{\upsilon^3}\left[m + \frac{n(1-\upsilon)}{Re}\right], \tag{11}$$

where $m = 1.75$ and $n = 4.2Re^{5/6}$ are constants, $\upsilon = 0.5$ is the catalyst bed void fraction, d_p is the catalyst diameter(m), μ_g is the gas viscosity, the gas specific heat capacity ρ_{pg} and the Reynold's number is $Re = \frac{Gd_t}{\mu_g}$ with d_t is the internal tube diameter (m). The gas velocity is calculated by

$$v_{pg} = \frac{G_{pg}}{\rho_{pg}}, \tag{12}$$

where G_{pg} is the mass velocity of the process gas.

Equation (6) is a classical example of a reaction-diffusion equation with a strong non-linearity and possibly stiff behavior. Such situations appear in a multitude of physical and in biological applications. In energy problems they appear, for instance, in bilayer organic photovoltaic devices [21]. They call for a careful numerical solution so as to avoid

instabilities and numerical error. In fact, dealing with stiff equations is a dignified problem in numerical analysis which attracted the attention of many researchers. See for example [9]. Our numerical solution of the coupled chemical and thermal problem is based on a third-order Runge-Kutta IMEX-SSP3(3,3,2) L-stable scheme. Such schemes are also used in hyperbolic problems in the presence of waves in atmospheric fields [16]. The Strong Stability Preserving (SSP) methods are numerical schemes that can be decomposed into a convex combination of Euler steps. This provides the stability preserving properties. The Implicit-Explicit (IMEX) approach relies on evaluating the stiff term of the equations with an explicit form, while the other terms are calculated by an implicit scheme [11]. The spatial resolution is obtained with second-order central difference schemes. The final result is an accurate and effective code for the determination of the temperature distribution inside the reformer tubes.

2.2. Furnace Side Modelling

The radiative model for simulating of the burner-box section is the Roesler flux-type model used by [7]. The governing equation is:

$$\frac{\partial^2}{\partial z^2} F = \alpha \left(\beta F + \gamma(T_{fg}) \right) \tag{13}$$

$$c_{p,fg} G_{fg} \frac{\partial}{\partial z} T_{fg} = 4K_a \left(F - E_{fg}(T_{fg}) \right) + Q(z) \tag{14}$$

where $c_{p,fg}$ is the specific heat at constant pressure of the flue gas and the energy $Q = Q(z)$ coming from the burners is typically assumed to be

$$Q(z) = q_0 \frac{6}{L} \frac{z}{L} \left(1 - \frac{z}{L} \right),$$

F is subject to homogeneous ($\frac{\partial}{\partial z}F = 0$) Neumann boundary conditions at the extremes $z = 0$ and $z = L$, and $T_{fg}(z = 0) = (F/\sigma)^{1/4}$. The values of α, β, γ are given by

$$\alpha = -\frac{2K_a + A_t + A_r}{2} \tag{15}$$

$$\beta = -(4K_a + 2\epsilon_t A_t) \tag{16}$$

$$\gamma = 4K_a E_{fg} + 2\epsilon_t A_t E_t \tag{17}$$

The flue gas mass velocity is obtained from

$$G_{fg} = \frac{M_w C_{fr}}{S_f} \tag{18}$$

where M_w is the total molar weight of the flue gas, C_{fr} is the combustion air flow rate and S_f is the furnace cross section area.

The solution of the furnace side is based on the numerical approximation of Equation (13) by a finite-difference method with the appropriate homogeneous Neumann boundary conditions coupled with the solution of Equation (14) by an implicit-explicit numerical solver for ordinary differential equations. The coupled nonlinear system of equations is solved by an iterative method that alternates between solving Equations (13) and (14). We set up a suitable iterative method which converges fairly fast to the solution. As usual, we start with an initial guess for F (typically a constant value) solve (the discretized) Equation (14) for T_{fg}, then we solve Equation (13) for F and so on, till convergence is reached. We notice that Equation (13) is (affine) linear in the unknown function F. This leads, by the finite difference method, to a sparse (almost tridiagonal) system which can be solved very fast and stably with standard linear algebra subroutines.

Several physical quantities used in our equations depend directly on the gas temperature and composition, such as specific heats, effective radial diffusivity, effective radial conductivity, viscosity and the thermal conductivity. We have used the well-accepted polynomial expansions given in Ref. [13]. The problem under consideration requires the solution of a complex system composed of two main parts. The outer one consists of the furnace and

the inner one consists of the tubes where the gas reforming process is taking place. The two parts are coupled and interact in a nonlinear form through Equation (1).

2.3. Flame Energy Estimation

The proof of the estimate given in Equation (2) starts by looking into the system of equations

$$\frac{\partial^2}{\partial z^2}F = \alpha\left(\beta F + \gamma(T_{fg})\right) \tag{19}$$

$$c_{p,fg}G_{fg}\frac{\partial}{\partial z}T_{fg} = 4K_a\left(F - E_{fg}(T_{fg})\right) + Q(z) \tag{20}$$

where the energy $Q = Q(z)$ delivered to the system from the burners is typically assumed to be [22]

$$Q(z) = q_0\frac{6}{L}\frac{z}{L}\left(1 - \frac{z}{L}\right). \tag{21}$$

Here, F is subject to homogeneous ($\frac{\partial}{\partial z}F = 0$) Neumann boundary conditions at the extremes $z = 0$ and $z = L$, and $T_{fg}(z = 0) = (F/\sigma)^{1/4}$. This delivers a steady state in which energy from the burners changes the temperature of the whole system, heating also the gas injected in the oven, instead of unphysical fixed temperatures. The values of α, β, and γ are given by

$$\alpha = -\frac{2K_a + A_t + A_r}{2}, \tag{22}$$

$$\beta = -\left(4K_a + 2\epsilon_t A_t\right), \tag{23}$$

$$\gamma = 4K_a E_{fg} + 2\epsilon_t A_t E_t. \tag{24}$$

In what follows we shall drop the indices fg in the temperature T_{fg}, G_{fg}, and c_{fg}, since such quantities till the end of this subsection make reference to the flue gas. We proceed by integrating Equation (20)

$$cG(T_{out} - T_{in}) = 4K_a\left(\int_{z=0}^{z=L} F dz - \int_{z=0}^{z=L} E_{fg} dz\right) + \int_{z=0}^{z=L} Q(z) dz\ ,$$

where T_{out} (T_{in}) refer, respectively to the output (input) temperatures of the flue gas. Thus, introducing, $q_0 := \int_{z=0}^{z=L} Q(z)dz$, we obtain

$$q_0 = cG\left(T_{out} - T_{in}\right) - 4K_a\left(\int_{z=0}^{z=L} F dz - \int_{z=0}^{z=L} E_{fg} dz\right) \ . \tag{25}$$

Next, we integrate (19) taking into account the boundary conditions

$$\beta \int_{z=0}^{z=L} F dz + \int_{z=0}^{z=L} 4K_a E_{fg} dz + 2\epsilon_t A_t \int_{z=0}^{z=L} E_t dz = 0 \tag{26}$$

and thus, substituting into Equation (25) we obtain

$$q_0 = cG(T_{out} - T_{in}) + 4K_a\left(\left(1 + \frac{4K_a}{\beta}\right)\int_{z=0}^{z=L} E_{fg} dz + \frac{2\epsilon_t A_t}{\beta}\int_{z=0}^{z=L} E_t dz\right) \ . \tag{27}$$

We now make use of (22)

$$\left(1 + \frac{4K_a}{\beta}\right) = -\frac{2\epsilon_t A_t}{\beta}$$

and thus

$$q_0 = cG(T_{out} - T_{in}) + 8\frac{K_a \epsilon_t A_t}{\beta}\left(\int_{z=0}^{z=L} (E_t - E_{fg}) dz\right) \ .$$

On the other hand, by the black-body radiation relation,

$$E_t = \sigma T_t^4 \text{ and } E_{fg} = \sigma T_{fg}^4 \ .$$

Thus, our task consists in approximating the integral

$$\text{Radiative} := \sigma \int_{z=0}^{z=L} (T_t^4 - T_{fg}^4) dz \ . \tag{28}$$

For that we introduce the (usually negative) temperature difference between the tube outer skin and of the flue gas

$$\Delta T := (T_t - T_{fg}) \ .$$

Under reasonable operating conditions the maximum change of $|\Delta T|$ would be much smaller

than T_t and T_{fg}. Thus, a good first order approximation to the integral in (28) is given by

$$\int_{z=0}^{z=L} (T_t^4 - T_{fg}^4) dz \approx \left(\int_{z=0}^{z=L} \Delta T dz \right) 4\overline{T_{fg}}^3 = L\overline{\Delta T} 4\overline{T_{fg}}^3 ,$$

where $\overline{T_{fg}}$ is taken as the average value of the flue gas temperature in the furnace, leading to Equation (2), namely:

$$q_0 \approx c_{fg} G_{fg} (T_{\mathrm{fg},out} - T_{\mathrm{fg},in}) + \frac{8\sigma K_a \epsilon_t A_t L}{\beta} \quad \overline{\Delta T} \quad 4\overline{T_{\mathrm{fg}}}^3 .$$

In words, the flame energy results in a temperature change of the flue gas between input and output, given by $c_{fg} G_{fg} (T_{fg,out} - T_{fg,in})$, and a radiative transfer between the flue gas and the tube. The quality of our analytic expression is verified in Table 1, Figure 2 and Figure 3, where our calibration scheme is graphically illustrated.

q_0 (W m^{-3})	ΔT (K)	$T_{fg}(z-0)$ (K)	T_{mean} (K)	$T_{fg}(z-L)$ (K)	T_{skin} (K)
21518	-200	1169	1224	1186	986
32278	-190	1338	1401	1348	1158
43037	-210	1421	1493	1428	1219
64555	-191	1667	1743	1668	1476
86074	-209	1786	1871	1784	1575

Table 1: Resulting notable temperatures for a given flame energy q_0. All other input parameters are given in Tables 2 and 3.

Note that the actual average temperature difference between the tube outer skin furnace and the flue gas for each energy flame value is approximately -200 K. Thus, we fix $\overline{\Delta T}$=-200K, select the central temperature $\overline{T_{fg}}$=1493 K and choose $T_{fg,in}$=1000 K.

This completely defines our calibration scheme connecting $T_{fg,out}$, which can be measured with the required energy flame q_0.

Note that Equation (2) can be rewritten as

$$q_0 = aT_{fg,out} + b \ , \tag{29}$$

and the averages provided by our numerical calculations combined with the input parameters given above lead to $a = 106.7$ and $b = -100688$, shown in the dashed (green) curve

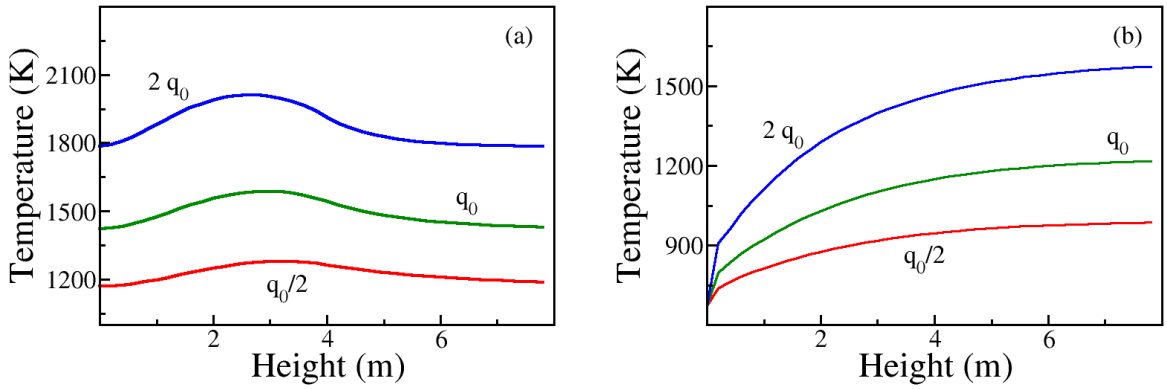

Figure 2: Temperature profile of a MIDREX reformer for different energy flame values described in Tab. 1. Here $q_0 = 43036.96\,(\mathrm{W\,m^{-3}})$. All other input parameters are given in Tables 2 and 3. The left panel presents the temperature curves in the furnace side of the reactor. The right panel has the temperature profile inside the reactor.

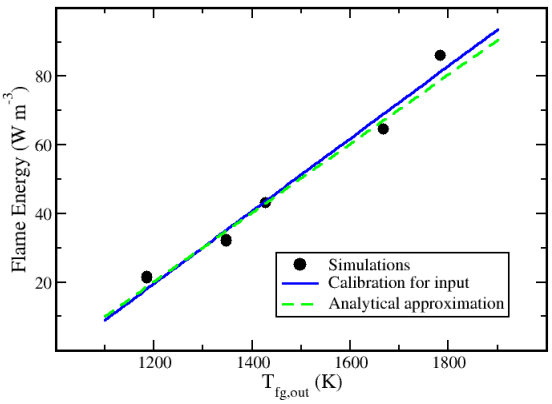

Figure 3: Calibration directly connecting the more easily measurable $T_{fg,out}$ to be used as input parameter with the required energy flame q_0. The symbols (black circles) are from Table 1, the solid (blue) line is the linear regression determining the best straight line connecting the points and the dashed (green) line is calculated with our calibration scheme defined by Equation (2).

of Figure 3. The linear regression for the calculated symbols (black circles) shown as a solid (blue) curve corresponds to $a = 105.79$ and $b = -107350$. The excellent agreement between our analytic expression determining the calibration scheme and the exact data calculated in our simulations, fully justifies using $T_{fg,out}$ as the input parameter determining how much energy is delivered by the burners to the system. Our global scheme allows

the calibration of each different burner system within the operation range of MIDREX reformers.

3. Results and Discussion

In this section we start with a direct application of the numerical algorithms, which were programmed in Octave [23], followed by a graphical solution of the energy/catalyst dichotomy. The input parameters used in each example are listed in Tables 2 and 3.

3.1. Model Validation

General operation data	
Furnace dimension	41 m x 15 m x 18 m
Total number of burners	168
Emissivity of tubes (ϵ_t)	0.85
Flame length (L_f)	4 m
Combustion air flow rate (C_{fr})	126390 Nm^3/h
Flue gas mass velocity (G_{fg})	0.045458 kg m^{-2} s^{-1}
Combustion air inlet temperature ($T_{fg,in}$)	873 K
Combustion air outlet temperature ($T_{fg,out}$)	1300 K
Average of the difference temperature ($\overline{\Delta T}$)	-200 K
Average flue gas temperature in the furnace ($\overline{T_{fg}}$)	1087 K

mol%	CH_4	H_2O	CO	H_2	CO_2	N_2
Fuel	6.79	6.11	23.77	43.95	17.76	0.9

Table 2: General operation conditions parameters following the work of Shayegan et al.[7]. Note that the input $\Delta T = -200$K e $\overline{T_{fg}} = 1086.5$K corresponds to flame energy $q_0 = 43037 \mathrm{Wm}^{-3}$.

Figure 4 is a reference for the direct solution of the problem and thus a direct model validation. Inside the reformer tubes we see an increase in temperature consistent with the heat exchange along the tube lengths and the molar fraction depicted confirm that the reactions are going in the expected direction, with a large production of H2 and CO. This figure defines the target CO concentration around 38%.

Input parameters	
Total number of tubes (N_t)	432
Reformer tubes inside diameter (d_t)	0.200 m
Reformer tubes outside diameter ($d_{t,out}$)	0.224 m
Thermal conductivity of tube (k_t)	90.9209 W m^{-1} K^{-1}
Length of reformer tubes (L)	8 m
Inert catalyst zone ($L - z$)	0 – 0.65 m
Active catalyst zone (z)	0.65 – 8 m
Catalyst density (ρ_B)	250 kg m^{-3}
Feed gas flow rate (F_{fr})	107122 N m^3 h^{-1}
Feed gas mass velocity (G_{pg})	1.6898 kg m^{-2} s^{-1}
Feed inlet temperature (T_{feed})	673 K
Inlet pressure of feed gas (P_{feed})	246 kPa

mol%	CH_4	H_2O	CO	H_2	CO_2	N_2
Feed	14.99	13.64	18.95	35.02	14.24	1.03

Table 3: Input parameters for the system under consideration. Refs. [7, 20]

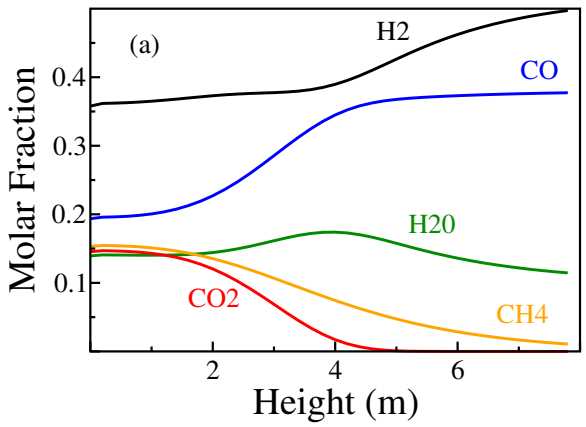

Figure 4: Molar fraction of the different gases along the height of the reformer tubes (left panel), using the parameters in Tables 2 and 3. Note the stabilization of the syngas (CO) concentration.

3.2. Catalyst vs Energy

The curves for the converted concentration of CO (syngas) tend to reach a plateau much before the end of the reformer tube. This indicates that on such plateaus, for a given set of temperatures, there is a minimum quantity of catalyst, that we call target catalyst length that delivers the desired syngas concentration. This is thus the first instance of our investigation of the interplay between energy and catalyst. In Figure 5 the amount of catalyst is changed in terms of its density and the energy input is varied through the

reactor inlet temperature, i.e. the temperature at which the process gas is injected in the reactor. The range of catalyst densities, namely $\rho_B = 250\,\mathrm{kg\,m^{-3}}$ to $\rho_B = 1016.4\,\mathrm{kg\,m^{-3}}$, correspond to values widely accepted in the literature [7, 24].

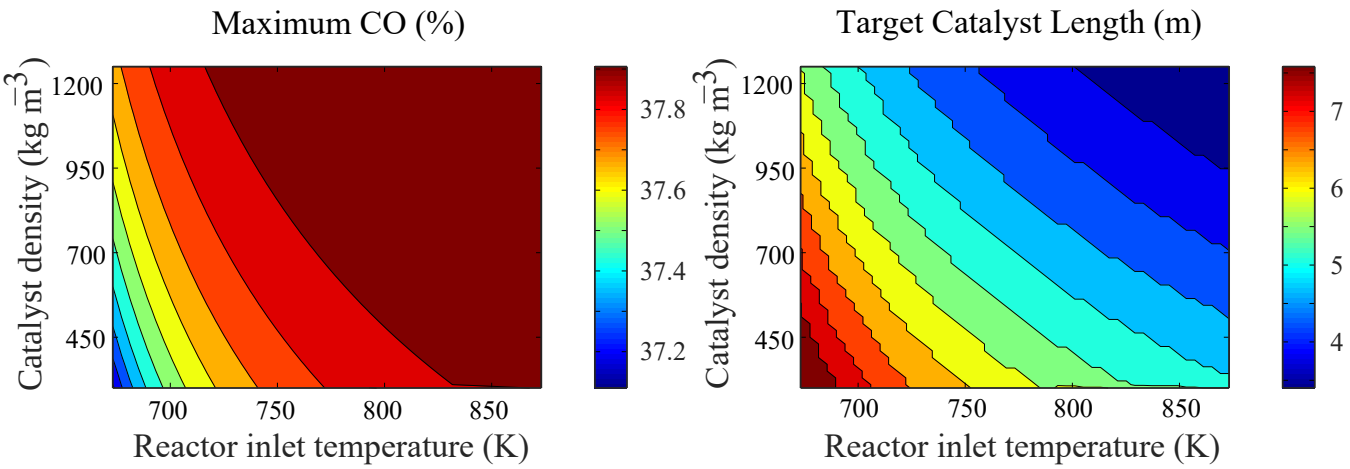

Figure 5: The left panel of this figure depicts how the maximum concentration of the main output reformer gas CO varies with respect to inlet temperature (T_{pg}) and catalyst density (ρ_B). All other input parameters are given in Tables 2 and 3. A graphical solution of how much catalyst is needed to reach the maximum output for (T_{pg},ρ_B) is given by the saturation length (y_s) in the right panel, since the tube cross section is constant.

In Figure 6 we complement this study by varying the inert zone while keeping all the other inputs and specifications. The inlet temperature is 843.15K and catalyst density is $1200\,\mathrm{kg\,m^{-3}}$. The left panel displays the concentration for the scenario where the catalyst is limited between 0.65 m and 4.0 m while the remaining of the reformer tube is inert. The right panel displays the situation where the catalyst starts at 4 m. The upshot being that one can minimize the catalyst expenditure while keeping the same output molar fraction of syngas. An assessment of the energy-catalyst interplay inside the reformer tubes is given in Fig. 7.

Figures 5, 6 and 7 show how we can clearly control energy injected through the process gas, but of course most of the energy is used in the ovens. Thus, Figure 8 illustrates how we can use our method to exploit the interplay between the energy flame input measured (q_0) and the amount of catalyst, measured by the length of the catalyst zone (L_c). Note that the same target CO concentration can be reached with low energy, high catalyst amount with

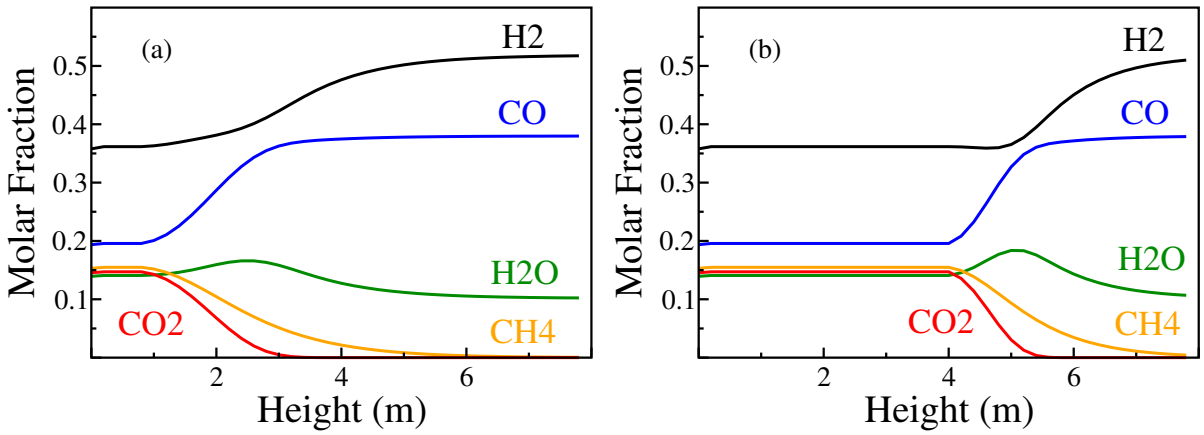

Figure 6: Gas concentration profiles inside the reformer tubes for two different catalyst and inert zones with inlet temperature $T_{pg} = 843.15$K and catalyst density $\rho_B = 1200\,\mathrm{kg\,m^{-3}}$. The left panel has inert zone in $0 - 0.65$ m and $4.0 - 8.0$ m and catalyst zone $0.65 - 4.0$ m. The right panel has inert zone in $0 - 4.0$ m and catalyst zone in $4.0 - 8.0$ m. All other input parameters are given in Tables 2 and 3. Note the possibility of using less active catalyst while still keeping the same end molar fraction of syngas.

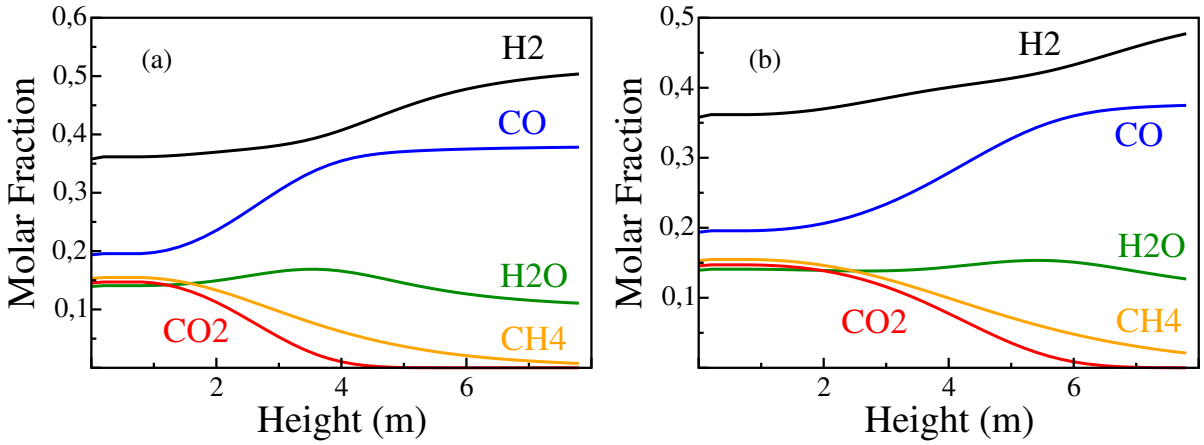

Figure 7: Gas concentration profiles inside the reformer tubes for two different catalyst zones and inlet temperature of process gas with catalyst density $\rho_B = 420\,\mathrm{kg\,m^{-3}}$. The left panel has inlet temperature $T_{pg} = 850$K, inert zone in $0 - 0.65$ m and $5.65 - 8.0$ m and catalyst active zone $0.65 - 5.65$ m. The right panel has inlet temperature $T_{pg} = 673.15$K, inert zone in $0 - 0.65$ m and catalyst active zone in $0.65 - 8.0$ m. All other input parameters are given in Tables 2 and 3.

q_0=47 KWm^{-3} and L_c 0.65 - 3.61 m (red dashed) compared with high energy, low energy amount with q_0=86 KWm^{-3} and L_c 0.65 - 6.47 m (blue solid curve). This completes our analysis of how resources can be efficiently manipulated in regions with low cost energy available, where a smaller quantity of catalyst can be used in contrast with locations with high energy costs per KWh, where the investment would be needed on the catalyst density/quantity.

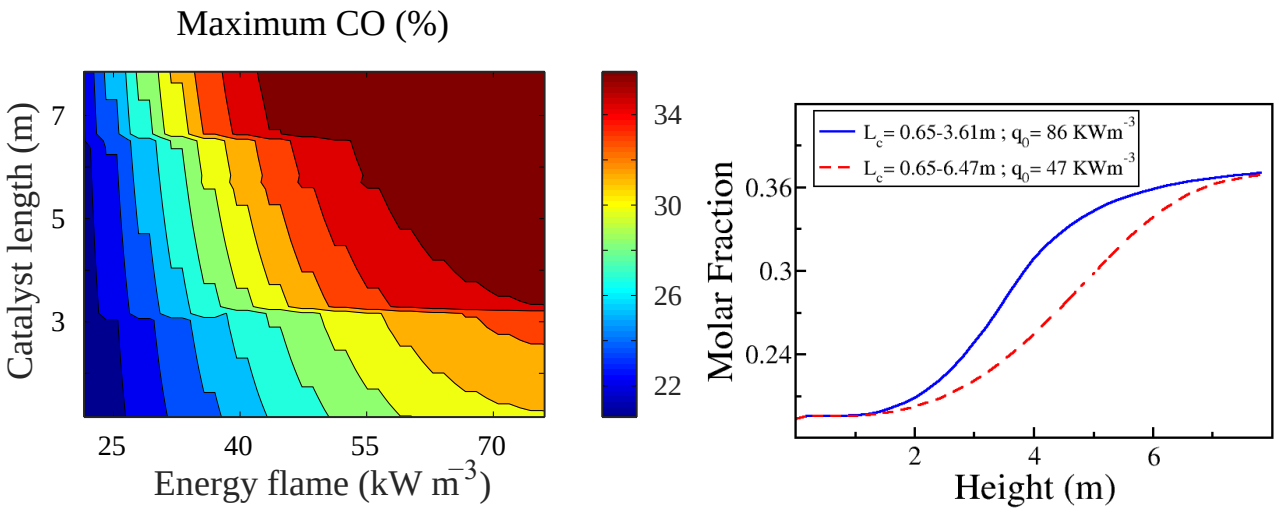

Figure 8: The panels depict how the target CO concentration can be reached for various combinations of energy flame (q_0) and amount of catalyst, measured by the length of the catalyst zone (L_c). The catalyst density is $\rho = 250$ Kg m^{-3}. All other input parameters are given in Tables 2 and 3. The solid (blue) line is for $L_c = 0.65$ - 3.61 m and $q_0 = 86$ KW m^{-3}, corresponding to high flame energy and small catalyst quantity. In contrast, the red (dashed) curve is for $L_c = 0.65$ - 6.47 m and $q_0 = 47$ KW m^{-3}, with low flame energy compensated by a large quantity of catalyst in the reformer tube.

4. Conclusion

In summary, this papers addresses outstanding issues regarding the MIDREX process. It shows how to decide between investing in either energy or catalyst amount to achieve production targets and how to express the energy input in terms of easily measurable temperatures. Our design tool leads to a flexible and modular computational implementation. It is capable of incorporating different material parameters while respecting the multiphysics and thermodynamical problem characteristics. It can be easily adapted to optimize the efficiency of other catalytic processes, with direct economic and environmental impacts.

Acknowledgements

We acknowledge the contribution of Eng. Luiz Claudio Dantas (LAMCA) who helped with multiple technical aspects of the Octave software and the skillful help of IMPA's artist Mr. Sergio R. Vaz with the graphical abstract. JPZ was supported by CNPq grants 302161 and 47408, and by FAPERJ under the program *Cientistas do Nosso Estado*. MFP was

supported by the Czech Science Foundation (GAČR) through grant No. 19-03765S and the EU H2020-Europe's resilience to crises and disasters program (H2020—grant agreement no. 832876).

References

[1] J. R. Rostrup-Nielsen, Catalysis and large-scale conversion of natural gas, Catalysis Today 21 (2-3) (1994) 257–267.

[2] Office of Energy Efficiency & Renewable Energy., Hydrogen production: Natural gas reforming., oEE Report (2019).

[3] Y. Zhang, S. Guo, Z. Tian, Y. Zhao, Y. Hao, Experimental investigation of steam reforming of methanol over la2cuo4/cuznal-oxides nanocatalysts, Applied Energy 254 (2019) 113022.

[4] K. Panagi, C. J. Laycock, J. P. Reed, A. J. Guwy, Highly efficient coproduction of electrical power and synthesis gas from biohythane using solid oxide fuel cell technology, Applied Energy 255 (2019) 113854.

[5] L. Lei, J. M. Keels, Z. Tao, J. Zhang, F. Chen, Thermodynamic and experimental assessment of proton conducting solid oxide fuel cells with internal methane steam reforming, Applied Energy 224 (2018) 280 – 288.

[6] M. T. Inc., 2017 World Direct Reduction Statistics (2018).
URL https://www.midrex.com/assets/user/news/MidrexStatsBook2017.5_.24_.18_.pdf

[7] J. Shayegan, M. M. Y. M. Hashemi, K. Vakhshouri, Operation of an industrial steam reformer under severe condition: A simulation study, The Canadian Journal of Chemical Engineering (2008) 86 (4).

[8] IEA GHG, Iron and steel ccs study (techno-economics integrated steel mill, iEAGHG Report, (2013) 2013/04.

[9] U. M. Ascher, S. J. Ruuth, B. T. R. Wetton, Implicit-explicit methods for time-dependent partial differential equations, SIAM Journal on Numerical Analysis 32 (3) (1995) 797–823.

[10] U. M. Ascher, S. J. Ruuth, R. J. Spiteri, Implicit-explicit runge-kutta methods for time-dependent partial differential equations, Applied Numerical Mathematics 25 (2) (1997) 151 – 167, special Issue on Time Integration.

[11] L. Pareschi, G. Russo, Implicit–explicit Runge–Kutta schemes and applications to hyperbolic systems with relaxation, Journal of Scientific Computing 25 (1) (2005) 129–155.

[12] S. Boscarino, L. Pareschi, On the asymptotic properties of imex runge–kutta schemes for hyperbolic balance laws, Journal of Computational and Applied Mathematics 316 (2017) 60 – 73.

[13] M. H. Wesenberg, Gas heated steam reformer modelling, Ph.D. thesis, Norwegian University of Science and Technology (2006).

[14] M. H. Wesenberg, J. Strohle, H. F. Svendsen, A study of the heating section of a gas heated steam reformer, International Journal of Chemical Reactor Engineering 5, (2007) A8.

[15] M. H. Wesenberg, H. F. Svendsen, Mass and heat transfer limitations in a heterogeneous model of a gas-heated steam reformer, Industrial & Engineering Chemistry Research 46 (3) (2007) 667–676.

[16] A. Rokhzadi, A. Mohammadian, M. Charron, An optimally stable and accurate second-order SSP Runge-Kutta IMEX scheme for atmospheric applications, Journal of Advances in Modeling Earth Systems 10 (1) (2018) 18–42.

[17] J. Xu, G. F. Froment, Methane steam reforming, methanation and water-gas shift: I. intrinsic kinetics, AIChE journal 35 (1) (1989) 88–96.

[18] C. P. Singh, D. N. Saraf, Simulation of side fired steam-hydrocarbon reformers, Industrial & Engineering Chemistry Process Design and Development 18 (1) (1979) 1–7.

[19] G. F. Froment, K. B. Bischoff, J. De Wilde, Chemical reactor analysis and design, Vol. 2, Wiley New York, 1990.

[20] F. Farhadi, M. Motemed Hashemi, M. Bahrami Babaheidari, Modelling and simulation of syngas unit in large scale direct reduction plant, Ironmaking & steelmaking 30 (1) (2003) 18–24.

[21] D. Brinkman, K. Fellner, P. A. Markowich, M.-T. Wolfram, A drift–diffusion–reaction model for excitonic photovoltaic bilayers: Asymptotic analysis and a 2d hdg finite element scheme, Mathematical Models and Methods in Applied Sciences 23 (05) (2013) 839–872.

[22] F. Roesler, Theory of radiative heat transfer in co-current tube furnaces, Chem. Eng. Sci. 22 (1967) 1325–1336.

[23] J. W. Eaton, D. Bateman, S. Hauberg, GNU Octave version 3.0.1 manual: a high-level interactive language for numerical computations, CreateSpace Independent Publishing Platform, 2009, ISBN 1441413006.
URL http://www.gnu.org/software/octave/doc/interpreter

[24] M. N. Pedernera, J. Piña, D. O. Borio, V. Bucalá, Use of a heterogeneous two-dimensional model to improve the primary steam reformer performance, Chemical Engineering Journal 94 (1) (2003) 29–40.